Journal of Quality Measurement and Analysis *JQMA* 22(1) 2026, 141-159
e-ISSN: 2600-8602 *http://www.ukm.my/jqma*
https://doi.org/10.17576/jqma.2201.2026.08

TRAJECTORY CONTROL OF A DELIVERY QUADCOPTER USING SELF-TUNING FUZZY-PID AND EXTENDED KALMAN FILTER

BELGIS AINATUL IZA, CHAIRUL IMRON & MARDLIJAH*

ABSTRACT

Quadcopter is a very popular technology because it is flexible in movement and has high maneuverability. However, Quadcopter has challenges in maintaining flight stability and trajectory stability in changing environments. The Proportional-Integral-Derivative (PID) control is less responsive because the parameters are set manually. Previous studies have attempted to combine Fuzzy-PID with Extended Kalman Filter (EKF). Previous approaches improved control but remained sensitive to disturbances. This study proposes an EKF-based Fuzzy-PID control where the PID parameters are adjusted automatically using Fuzzy and EKF functions to adjust the Fuzzy parameters adaptively. The proposed control method minimizes angular and linear errors under various conditions. From the simulation, the system is able to follow the reference with high precision, with position errors of x, y, z axis are 0.15 m, 0.12 m, and 0.10 m respectively. The low z-axis error indicates stable altitude control. Under disturbances, the average position error increases by only about 0.09 m on each axis. It shows that the EKF-based Fuzzy-PID controller has effective and adaptive performance in uncertain environments.

Keywords: quadcopter; fuzzy-PID; Extended Kalman Filter; self-tuning PID; adaptive control

1. Introduction

Fuzzy control is often used for uncertain and nonlinear systems (Pandey *et al.* 2022), so this control can be used as an alternative to designing a simple but effective control system (Şahin & Ulu 2023). Fuzzy logic can be used for complex nonlinear systems (Mardlijah *et al.* 2023), but fuzzy has disadvantages, such as being slow in achieving the desired response time and oscillations that cannot be eliminated. The problems caused by fuzzy logic can be overcome using PID (Nguyen *et al.* 2025; Zhu *et al.* 2022). The PID controllers help each other by combining the values of Ki, Kp, and Kd to obtain a stable output response and minimize oscillations at the set point (Issa *et al.* 2025; Wang *et al.* 2022). Here, proportional gain (Kp) is used to give a direct response to the the current error, integral gain (Ki) is used to eliminate long-term errors by accumulating the values of previous error, while derivative gain (Kd) is used to dampen rapid changes in errors, thus it results in a more stable system. Fuzzy and PID combination needs to be done so that the system is able to minimize errors, get the desired set point, and be able to get a faster response time to stabilize the system even though it is disturbed.

In recent periods, Fuzzy-PID has been the focus of several researchers in many fields (Nguyen *et al.* 2025; He *et al.* 2025; Aydenlou & Subasi 2025). However, it has weaknesses. The first weakness is the problem of parameter tuning in the controller (Somwanshi *et al.* 2019). Manual adjustment is still done in the research, so it is difficult to apply in various operating conditions. This limits the ability of the controller to be used widely in dynamic environments. The second weakness is that there is no pattern for adjusting the input-output of fuzzy systems (Arghavani *et al.* 2017). As a result, the system becomes less reliable in the face of uncertainty or nonlinear characteristics. This is because the mapping between system conditions and controller actions becomes inconsistent when the environment changes. The last weakness is the weakness in defining optimal rules, which results in limited controller effectiveness (Taghavifar 2021). This problem becomes more complex as the number of rules increases, increasing the complexity of the system without guaranteeing performance improvement. The rule base is unable to respond effectively to disturbances in real time without an adaptive implementation.

A method for adjusting membership functions (MFs) is needed to decrease errors and enhance stability. One of the effective methods for improving fuzzy logic performance is the Extended Kalman Filter (EKF) (Şahin & Ulu 2023; Oloo 2021; Odry *et al.* 2020). Research by Szedlak-Stinean *et al.* (2022) utilized the Extended Kalman Filter and a Takagi-Sugeno Fuzzy Observer to validate the two nonlinear estimation approaches. Gautam and Ha (2013) discussed Fuzzy-PID control based on EKF on Quadcopter and Zaman *et al.* (2025) applied Hybrid Extended Kalman Filter and Fuzzy Logic System for Autonomous Surface Ships, however, their methods still depend on fixed membership function. In contrast, this study uses EKF to set adaptability the parameters of fuzzy, and then the self-tuning fuzzy was used to obtain the PID gain, providing a better trajectory control in unpredictable environments. In addition, Honarbari *et al.* (2021) applied the strategy of maximum power point tracking by using EKF to determine unpredictable parameters and by using fuzzy logic control to control generator speed.

Although EKF has been widely used with fuzzy, the method still needs to be further developed. Seeing the importance of improving control performance, this study develops a Fuzzy-PID control design where the Fuzzy-PID parameter setting uses a robust Extended Kalman Filter, which produces a stable response to a changing environment. In this study, fuzzy parameters were estimated using the EKF algorithm, and the results of fuzzy parameter tuning were used to adjust the PID gain. Before estimating the state using EKF, the measurement model need to be linearized.

The novelty of this research lies in the development of a Fuzzy-PID controller with automatic tuning integrated with the Extended Kalman Filter (EKF) to improve the stability and control of the quadcopter trajectory under disturbance conditions. Different from previous studies, this method does not depend on either physical sensors or Global Positioning System (GPS) but uses state estimation through EKF and applies fuzzy logic to dynamically adjust PID parameters based on errors from 12 state variables. This integration enhances robust and adaptive control performance in uncertain environments.

The literature review in this section is structured thematically, covering preliminary studies on the application of conventional PID control on quadcopters, the development of fuzzy logic-based controllers to improve system adaptability, and the application of EKF in state estimation. Furthermore, the previously developed combination of Fuzzy-PID and EKF is discussed to demonstrate the uniqueness of the method proposed in this study.

The paper contains: First, it presents the introduction. Second, it expresses the detailed kinematics and dynamics model of quadcopter. Third, it explains the control system of Fuzzy-PID based on EKF. Fourth, it displays the results. The last is conclusion and recommendations for further research.

2. Mathematical Model

In this paper, a quadcopter drone is chosen as the research subject. Quadcopter is assumed as:

(1) The equation of motion formulated in quadcopter is body-fixed.
(2) The axis of body frame is located on the axis of inertia central.
(3) The motion of the quadcopter is observed while hovering.
(4) The quadcopter is observed while loading the load but is not observed until sending the goods.
(5) The payload is solid with a maximum mass of 5 kg.
(6) The payload is placed below and attached to the quadcopter.
(7) The controlled motion is the quadcopter maneuver motion, namely the angular velocity, the linear velocity, and acceleration.

From the Euler and Newton's second law, the following linear and angular equations are obtained (Abdelhay & Zakriti 2019). The subscript symbol 'B' in Eqs. (1)-(2) indicates that the

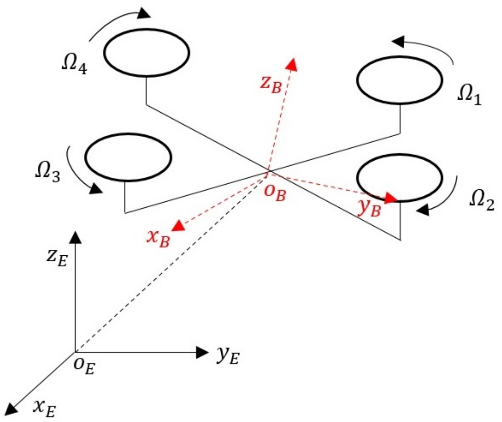

Figure 1: Coordinate on quadcopter (Chang *et al.* 2024).

frame of reference is the body-frame (B-frame), attached to the body of the quadcopter.

$$F^B = mI\dot{v}^B + \omega^B \times mv^B \tag{1}$$
$$\tau^B = I\dot{\omega}^B + \omega^B \times I\omega^B \tag{2}$$

where F^B notates the force (N); τ^B express the torque (Nm); m symbolize the quadcopter mass (kg); the quadcopter linear and angular velocity are notated as v^B and ω^B; I describes the quadcopter inertia matrix (Nms^2).

Earth and body frame are required to define quadcopter state when the kinematic describes. The matrix of rotation is written in Eq. (3).

$$R_\Theta = \begin{bmatrix} c_\psi c_\theta & -s_\psi c_\phi + c_\psi s_\theta s_\phi & s_\psi s_\phi + c_\psi s_\theta s_\phi \\ s_\psi c_\theta & c_\psi c_\phi + s_\psi s_\theta c_\phi & -c_\psi s_\phi + s_\psi s_\theta c_\phi \\ -s_\theta & c_\theta s_\phi & c_\theta c_\phi \end{bmatrix} \tag{3}$$

Furthermore, the transformation matrix is described in the following equation.

$$T_\Theta = \begin{bmatrix} 1 & s_\phi t_\theta & c_\phi t_\theta \\ 0 & c_\phi & -s_\phi \\ 0 & \frac{s_\phi}{c_\theta} & \frac{c_\phi}{c_\theta} \end{bmatrix} \tag{4}$$

Symbol s, c, and t are the notations for the trigonometric functions sin, cos, and tan. Symbol ϕ, θ, ψ indicate roll, pitch and yaw angle, respectively. The coordinate transformation on the quadcopter is displayed in Figure 1.

The direction of the quadcopter's motion is affected by the velocity of its four rotors. The difference in rotor velocity affects the amount of lift and torque. Then, U_1 is defined as the total thrust, U_2 notates the roll torques, U_3 represents the pitch torques, and U_4 describes the yaw torques formed by the propeller rotation. The equations are written as follows.

$$\begin{bmatrix} U_1 \\ U_2 \\ U_3 \\ U_4 \end{bmatrix} = \begin{bmatrix} C_t(\Omega_1^2 + \Omega_2^2 + \Omega_3^2 + \Omega_4^2) \\ C_t l(-\Omega_2^2 + \Omega_4^2) \\ C_t l(-\Omega_1^2 + \Omega_3^2) \\ C_m(-\Omega_1^2 + \Omega_2^2 - \Omega_3^2 + \Omega_4^2) \end{bmatrix} \tag{5}$$

The length between the rotor to the center of the quadcopter is symboled as l; C_t expresses thrust coefficient; C_m is the moment coefficient; and Ω_i is the rotational velocity of each four rotors. The speeds of the four propellers are described as follows.

$$\Omega = \Omega_2 + \Omega_4 - \Omega_1 - \Omega_3 \tag{6}$$

The kinematic equations for the translation motion of the quadcopter in the E-frame is obtained from rotation matrix multiplication in Eq. (3) with vector (u, v, w), which is written as below.

$$\begin{cases} \dot{x} = uc_\psi c_\theta + v(-s_\psi c_\phi + c_\psi s_\theta s_\phi) + w(s_\psi s_\phi + c_\psi s_\theta s_\phi) \\ \dot{y} = us_\psi c_\theta + v(c_\psi c_\phi + s_\psi s_\theta c_\phi) + w(-c_\psi s_\phi + s_\psi s_\theta c_\phi) \\ \dot{z} = -us_\theta + vc_\theta s_\phi + wc_\theta c_\phi \end{cases} \tag{7}$$

The multiplication of translation matrix in Eq. (4) and vector (p, q, r) result in the kinematic equations for the angular motion of the quadcopter in the E-frame coordinate system.

$$\begin{cases} \dot{\phi} = p + qs_\phi t_\theta + rc_\phi t_\theta \\ \dot{\theta} = qc_\phi - rs_\phi \\ \dot{\psi} = q\frac{s_\phi}{c_\theta} + r\frac{c_\phi}{c_\theta} \end{cases} \tag{8}$$

The variables $u,\ v,\ w$ and $p,\ q,\ r$ represent the velocities of linear and angular in three directions in the B-frame coordinate system; symbol $\dot{x},\ \dot{y},\ \dot{z}$ and $\dot{\phi},\ \dot{\theta},\ \dot{\psi}$ are the linear velocities and angular velocities in the E-frame.

Dynamic model in B-frame coordinate system, which consists of force and torque equations expressed in Eqs. (1) and (2), is described in more detail in these equations.

$$\begin{cases} \dot{u} = vr - wq + gs_\theta \\ \dot{v} = wp - ur - gc_\theta s_\phi \\ \dot{w} = uq - vp - gc_\theta s_\phi + \frac{U_1}{m} \end{cases} \tag{9}$$

$$\begin{cases} \dot{p} = \frac{(I_y - I_z)}{I_x} qr - \frac{J_r}{I_x} q\Omega + \frac{U_2}{I_x} \\ \dot{q} = \frac{(I_z - I_x)}{I_y} pr + \frac{J_r}{I_y} p\Omega + \frac{U_3}{I_y} \\ \dot{r} = \frac{(I_x - I_y)}{I_z} pq + \frac{U_4}{I_z} \end{cases} \tag{10}$$

Parameter J_r represents the rotor moment of inertia; I illustrate the inertia moment about the three axes; m is the quadcopter mass; U_1,U_2,U_3,U_4 is the trhust and torque expresses in Eq. (5); and Ω is the velocity of propellers described in Eq. (6).Then, the parameter values used in the quadcopter system are adopted from Chang *et al.* (2024).

The kinematic and dynamic models in Eqs. (7)-(10) are changed into $\dot{X} = f(X, U)$ state space. The state vector X represents the system condition and consists of 12 variables, namely linear position (x, y, z), linear velocity (u, v, w), angular velocity (p, q, r), and angular position roll, pitch, yaw (ϕ, θ, ψ). The control input vector U consist of the main control signals: $U1$ (thrust), $U2$ (roll torque), $U3$ (pitch torque), and $U4$ (yaw torque). The vectors X as well as U are defined in following equations.

$$X = [x \quad y \quad z \quad u \quad v \quad w \quad p \quad q \quad r \quad \phi \quad \theta \quad \psi]^T \tag{11}$$

$$U = [U_1 \quad U_2 \quad U_3 \quad U_4]^T \tag{12}$$

Table 1: Stability time

State	x	y	z	u	v	w	p	q	r	ϕ	θ	ψ
Time	3.96	3.32	5.53	4.34	3.60	7.09	2.08	3.88	3.63	3.29	3.59	3.28

then, the vector X in Eq. (11) is assumed to be

$$X = [x_1 \quad x_2 \quad x_3 \quad x_4 \quad x_5 \quad x_6 \quad x_7 \quad x_8 \quad x_9 \quad x_{10} \quad x_{11} \quad x_{12}]^T \tag{13}$$

After the system is changed into $\dot{X}$, the following process is to obtain a linear system of equations. Linearization of the system can be done through Taylor series expansion around the equilibrium point. According to Mellodge (2016), the general form of Taylor series expansion up to order N involves the Jacobian matrix and is written as follow.

$$J(X^*) = \begin{bmatrix} \frac{\partial f_1}{\partial X_1} & \cdots & \frac{\partial f_1}{\partial X_N} \\ \vdots & \ddots & \vdots \\ \frac{\partial f_N}{\partial X_1} & \cdots & \frac{\partial f_N}{\partial X_N} \end{bmatrix}$$

A quadcopter's linearized dynamic system modeling is written below

$$\dot{X} = AX + BU, \tag{14}$$
$$Y = CX + DU, \tag{15}$$

where X is the state vector represented in Eq. (13), $\dot{X}$ is the derivative of the state vector, U is the vector of input represented in Eq. (12), Y is the vector of output, and A, B, C, and D are the system dynamics matrix, input matrix, output matrix, and direct transmission matrix, respectively.

After the linearization results are obtained, a system analysis will be carried out in the form of a test of stability, controllability, and observability. Stability analysis is critical to determine whether the system remains in a safe condition under the influence of the designed control. The controllability test determines whether the system can be moved as desired. At the same time, the observability test helps assess whether the system can be estimated from the measured output.

In deciding the system stability, we can use the roots λ of the system obtained from the matrix A in Eq. (14). In this study, stability analysis was carried out using the eigenvalue approach presented as follows (Jiang 2022).

$$det(\lambda I - A) = 0 \tag{16}$$

By using Eq. (16), it is obtained that the eigenvalue is 0 with an algebraic multiplicity of 12 and a geometric multiplicity of 12. Conditions for a stable system (Wang *et al.* 2017): 1) real eigenvalues are zero, 2) algebraic multiplicity equals geometric multiplicity. Since it meets both criteria, so the system is stable. The results of this stability also match the Figure 2 in which the stability time is shown in the Table 1. Figure 2 illustrates that the state vector x consisted of 12 variables reaches stability after few seconds. Details of the stability time (in second) of each state are shown in the Table 1.

The controllability test requires matrices A and B obtained from Eq. (14) and can be checked by this controllability matrix (Lalwani *et al.* 2006).

$$M_c = [B \quad AB \quad A^2B \quad ... \quad A^{11}B] \tag{17}$$

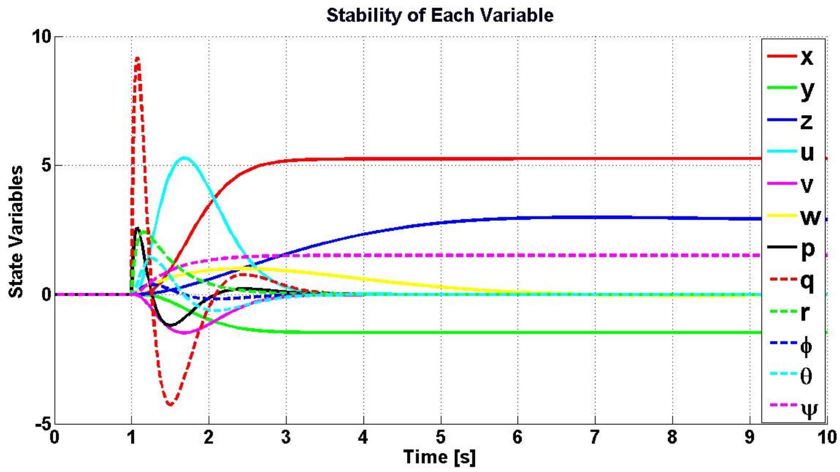

Figure 2: System stability

By using Eq. (17), we obtain the rank $M_c = 12$, which is same as state vector order. Therefore, the dynamic system can be controlled.

Matrices A and C from Eq. (14) and (15) are needed for the observability test. The observability is analyzed by finding the rank of the observability matrix expressed below (Lalwani *et al.* 2006).

$$M_o = [C \quad CA \quad CA^2 \quad \ldots \quad CA^{11}]^T \tag{18}$$

Based on the formula in Eq. (18), the value of rank is 12, so it can be concluded that the system can be observed. Since it is stable, controlled, and observed, it can be guaranteed to be controlled and monitored effectively so that control design and estimation can be applied.

3. Control System Architecture

After obtaining mathematical models, it is possible to design Fuzzy-PID controllers and EKF in a Simulink block to stabilize the quadcopter position. Designing the control system requires identifying the manipulable signals. In order to obtain optimal response results, the control parameters are tuning so that the output response is obtained as expected when determining the design criteria. PID gain is tuned by using fuzzy. The parameter of fuzzy is estimated by utilizing EKF. To test the control design, a disturbance is required when the quadcopter is traveling along the track. This aims to determine the response results from the quadcopter when it is disturbed whether it can still maintain its attitude while traveling along the trajectory or vice versa. In the simulation, a random disturbance type resembles wind to represent the continuous turbulence of the environment. This disturbance is more suitable for those that occur continuously rather than momentary disturbances such as steps or impulses. The disturbance is applied to all translational and rotational acceleration axes to represent realistic quadcopter flight conditions.

In the waypoint navigation system, the attitude and position are stabilized using Fuzzy-PID. The method of tuning here is used to determine Kp, Ki, and Kd parameters. Because the plant parameters are always changing according to the situation, the Fuzzy-PID here is expected to be able to maintain the stability of the quadcopter's motion when doing lateral motion, along the desired trajectory. The block of Fuzzy-PID controller is shown in Figure 3.

In the Fuzzy-PID, the inputs of fuzzy is error signal $e(t)$ and the derivative of the error $de(t)$ while the outputs is gains of PID (Kp, Ki, Kd). According to Nippatla and Mandava (2025),

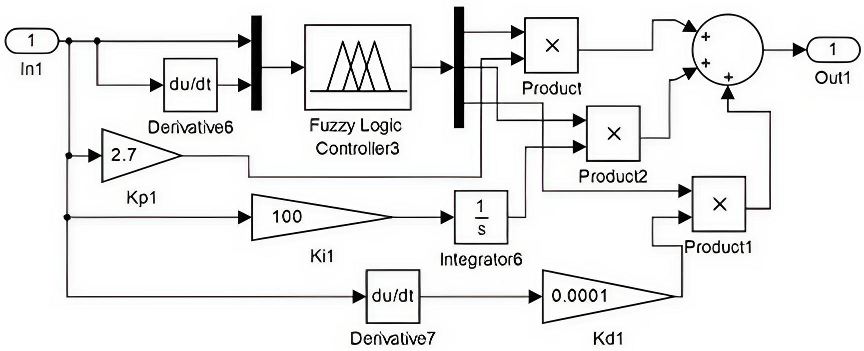

Figure 3: The Fuzzy-PID

PID control is defined as

$$u(t) = K_p e(t) + K_i \int e(t)dt + K_d \frac{de(t)}{dt}. \tag{19}$$

The parameter Kp, Ki, Kd are tuned based on the error and its derivative by using a fuzzy inference system. The fuzzy system uses triangular membership functions and 3×3-based fuzzy rules to adaptively determine control parameter values.

The input error value range is [-0.5 0.5] and [-0.025 0.025] for the derivative of the error. This range is the plant error limit which is designed from the fuzzy systematic method, so that later when the system is running, the controller keep the stability of the quadcopter's motion. The fuzzy inputs use a triangular membership function. The input variables e(t) and de(t) used are tree fuzzy set members, namely NB(Negative Big), N(Netral), and PB(Positive Big). In designing the controller, 9 fuzzy rule bases have been obtained for the tree members of the set. Referring to Truong and Ahn (2011) and Gautam and Ha (2013), Fuzzy-PID control uses triangular membership function because it is simple and commonly used. Although the initial fuzzy rules are designed manually, further adjustments are made adaptively by the EKF algorithm which updates the scale and influence of each rule and membership function. This is intended to reduce subjectivity and improve the adaptive performance of the system in dealing with uncertain conditions. The range of output parameter variables is Kp =[0.9;1.1], Ki =[0.9;1.1], and Kd=[0.9;1.1]. The parameters range are tuned by using PID simulation to get a possible rule base with efficiency. The output variables gain Kp, gain Ki, and gain Kd used are tree members of fuzzy support set. The membership functions for the controller parameter values Kp, Ki, and Kd have the same characteristics of mapping variables, namely PS (Positive Small), P (Positive), and PB (Positive Big).

The fuzzy parameter is estimated by EKF. The signal tracking is from the input reference trajectory. EKF estimates the state x using the u input system and y output system. The estimated state of system x is linear and angular position as well as linear and angular velocity. For more detail, the algorithm of EKF is illustrated in Figure 4. After estimating the state, the next process calculates the optimal control using the Linear Quadratic Regulator (LQR) method. LQR is defined as a state-feedback-based controller that is capable of minimizing the cost function to achieve optimal performance. Then, the signal and its derivative on the tracking setpoint are differentiated with two estimated states to gain the signal of error e and $\dot{e}$. These signals are back processed into Fuzzy-PID to calculate the input of control u. The structure of EKF is illustrated in Figure 5.

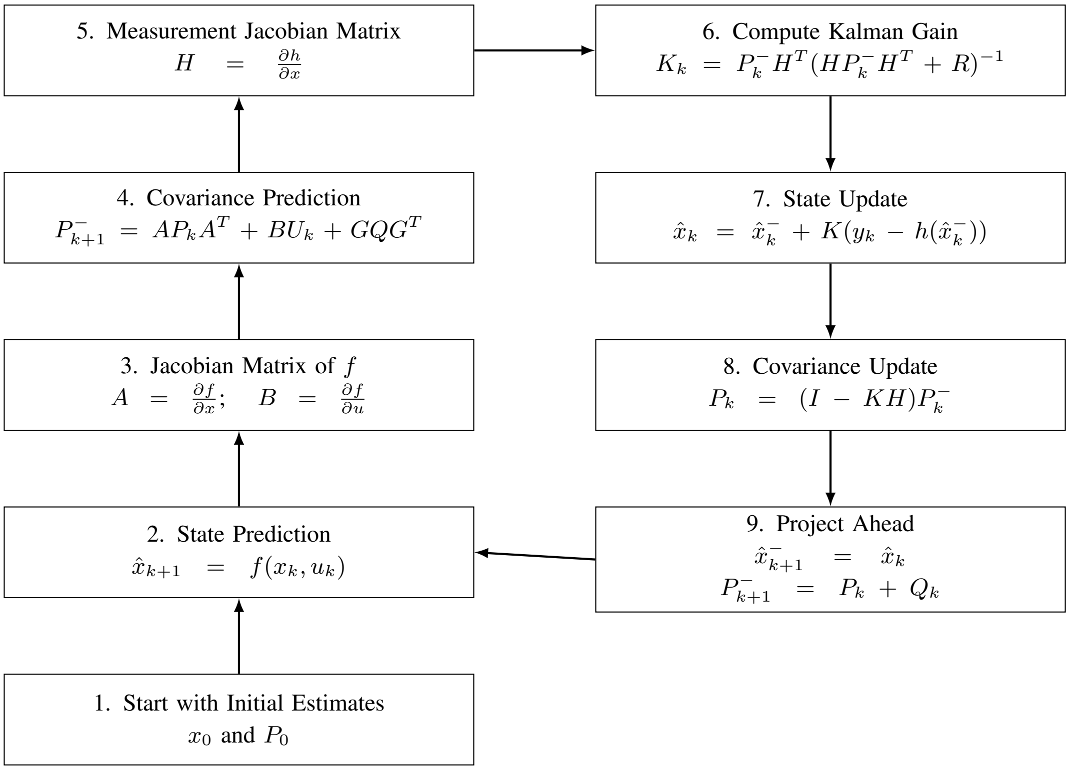

Figure 4: Extended Kalman Filter algorithm flowchart (Iza *et al.* 2022)

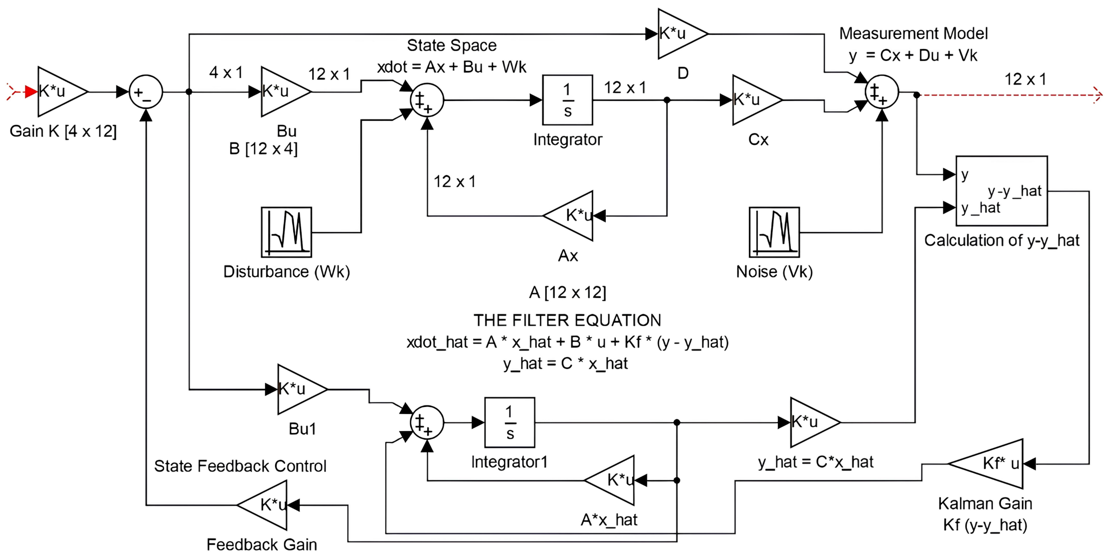

Figure 5: The structure of EKF

4. Experiments and Results

The system control simulation in this study uses Matlab software. The combination of Fuzzy-PID Controller and EKF are designed by using Simulink, demonstrated in Figure 6. The u

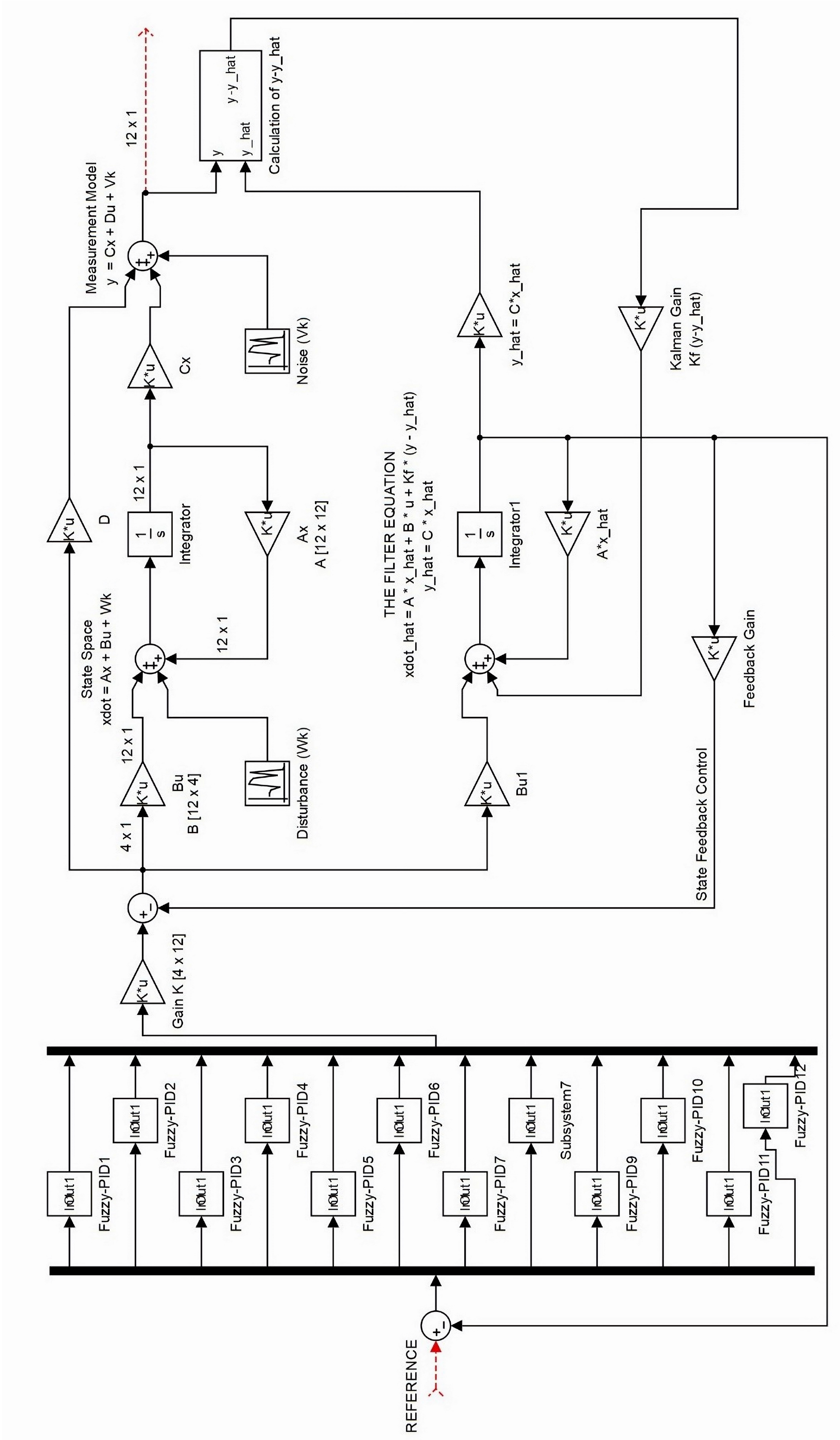

Figure 6: The Fuzzy-PID based on EKF

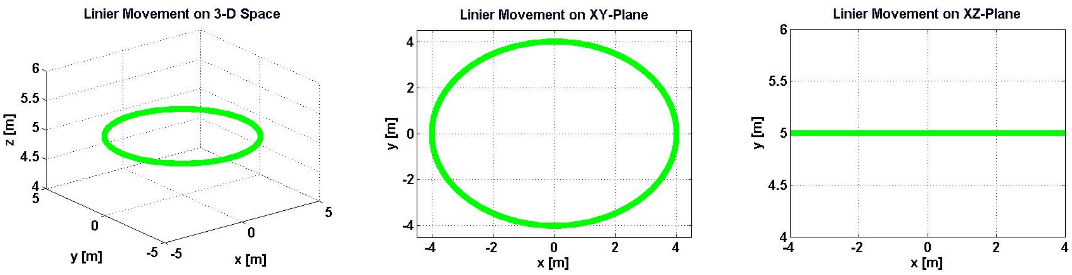

(a) (b) (c)

Figure 7: Reference path - circle on a horizontal plane: (a) 3D, (b) xy, (c) xz

control in the system is intended to get output as close as possible to the desired reference. The target position and trajectory in this study are viewed in Figure 7. Figures 8-12 show the performance of Fuzzy-PID controller based EKF. In order to evaluate the control system robustness, an external disturbance is applied to all translational and rotational states of the quadcopter in the form of a Gaussian random signal with a mean of zero, a variance of 1, and a sample time of 0.01 seconds. This stochastic disturbance is applied in all simulation scenarios shown in Figures 8-12.

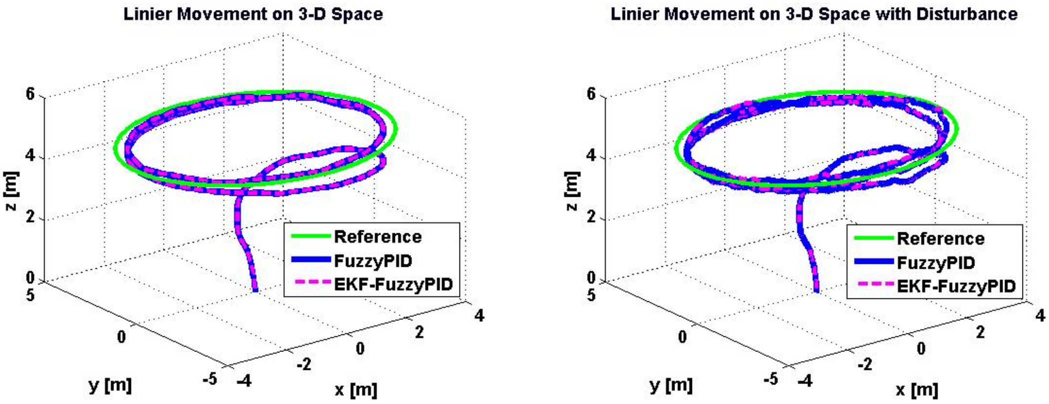

(a) (b)

Figure 8: Trajectory tracking on 3D: (a) without disturbance, (b) with disturbance

The performance of the EKF-FuzzyPID control system in three-dimensional space is demonstrated in Figure 8. In Figure 8a, a condition without disturbance, the EKF-FuzzyPID control system can follow the reference trajectory precisely. The position error for the x,y,z axis are 0.15 m , 0.12 m, and 0.10 m respectively. On the other hand, Figure 8b illustrates the performance of the control system with disturbance. Although deviation increase at the beginning, the control system adapt quickly and returns to reach the reference. The average position error increases for about 0.09 m for each axis.

Figure 9 shows that the EKF-FuzzyPID control system on the quadcopter has various performance depending on the disturbance applied. In the undisturbed condition, the overshoot of the yaw angle is relatively small (2.5050%) and the settling time is 16.7819 seconds. The steady-state errors for roll, pitch, and yaw are 0.3585, 0.1000, and 0.0031, respectively, meaning that the system is able to reach the reference value with a small final error, especially in the yaw angle. However, in the disturbed condition, the overshoot of roll and pitch remains undefined (Inf), while the overshoot of yaw increases significantly to 22.2782%, indicating the sensitivity of the system to disturbances. The settling time for all angles is undefined (NaN), indicating that the system has difficulty in achieving stability under disturbed conditions. However, the steady-state error at all three angles decreases compared to the undisturbed condition, which is 0.2734 for roll, 0.0655 for pitch, and 0.0584 for yaw. This shows that even though the system has large overshoot and undefined settling time under disturbed conditions, the system can still achieve smaller steady-state errors in roll and pitch, but experiences an increase in error in yaw.

In the case without disturbance (Fig. 9a–c), EKF-Fuzzy-PID has a much smaller overshoot than conventional Fuzzy-PID. For example, in Figure 9a (Roll), the overshoot of Fuzzy-PID is estimated to be about 3.5 rad, more than 4 times that of EKF-Fuzzy-PID which is only 0.8 rad. From the aspect of settling time, Fuzzy-PID does not seem to achieve stability in all cases, while EKF-Fuzzy-PID is able to reach a steady state in a relatively short time, although the disturbance is not completely eliminated. The final error in Fuzzy-PID is relatively high due to the continuous oscillation, while in EKF-Fuzzy-PID, the error value at the end point is much smaller and tends to converge closer to the reference value. In terms of quality, the response of EKF-Fuzzy-PID is much smoother without sharp oscillations, as shown by Fuzzy-PID. The disturbance rejection capability is also seen in Figure 9d–f, where the EKF-Fuzzy-PID is able to return to the reference quickly with minimal oscillation, while the Fuzzy-PID remains oscillating and fails to stabilize.

The EKF-Fuzzy-PID control analysis at the angular velocity of the quadcopter shown in Figure 10 shows significant differences between the conditions without disturbance and with disturbance. In the undisturbed system, the overshoot at the angular velocity is undefined (Inf), indicating an uncontrolled response at the initial stage. The settling time for roll is 19.9389 seconds, indicating the time for the system to attain a stable state, while the settling time for pitch and yaw is undefined (NaN), indicating instability or difficulty in achieving stability at both angles. The steady-state errors for roll, pitch, and yaw are 0.0990, 0.3581, and 0.1546, reflecting the error at steady state with a relatively small value for roll, but larger for pitch and yaw. In the condition with disturbance, the overshoot remains undefined (Inf) at all three angles, but the settling time for roll is slightly better with a value of 19.8944 seconds, which is almost the same as the undisturbed condition. Settling time for pitch and yaw is still undefined. Steady-state error for roll increases to 0.1422, for pitch to 0.3153, and for yaw decreases to 0.0881, indicating that although disturbances increase steady-state errors in roll and pitch, yaw shows improved performance with smaller steady-state errors. Overall, although the EKF-FuzzyPID system is not completely stable under disturbance conditions, it still shows the ability to reduce steady-state errors, especially in yaw.

In visual observation under undisturbed conditions (Fig. 10a–c), Fuzzy-PID controller shows large fluctuations in all angular velocity components, reflecting a rough and less stable response. In contrast, the EKF-Fuzzy-PID (pink line) consistently produces a smoother response, with smaller oscillation amplitudes and closer to the reference. The EKF-Fuzzy-PID response also moves to the reference faster and has lower noise compared to the Fuzzy-PID, which shows sharp fluctuations. Under disturbed conditions (Fig. 10d–f), the EKF-Fuzzy-PID control is proven to be more robust to disturbances: the system remains close to the reference with minimal variation, although there is a transient peak immediately after the disturbance is applied.

Figure 11 shows the performance of the EKF-FuzzyPID control system at x, y, and z positions that vary depending on the disturbance conditions. In the undisturbed system, the overshoots are 0.2804% in x, 123.7691% in y, and 1.1578% in z, with the y-axis showing very high overshoot, indicating a very uncontrolled system response in that axis. The settling times are undefined (NaN) in the x and y axes, indicating instability or difficulty in reaching a steady state in both axes. However, the settling time for z is 8.5175 seconds, indicating that the system is quite capable of achieving stability in the z axis even though the fault still exists. The steady-state errors are 2.7063, 1.8960, and 0.0082 for thee axis, indicating relatively large final position errors in the x and y axes, while in the z axis, the steady-state error is very small, indicating more accurate control of the position. Under the disturbance condition, the overshoot in all three axes increases, with x becoming 4.0022%, y becoming 128.9149%, and z becoming 3.0951%, indicating that the disturbance causes the system response to be more extreme, especially in y.

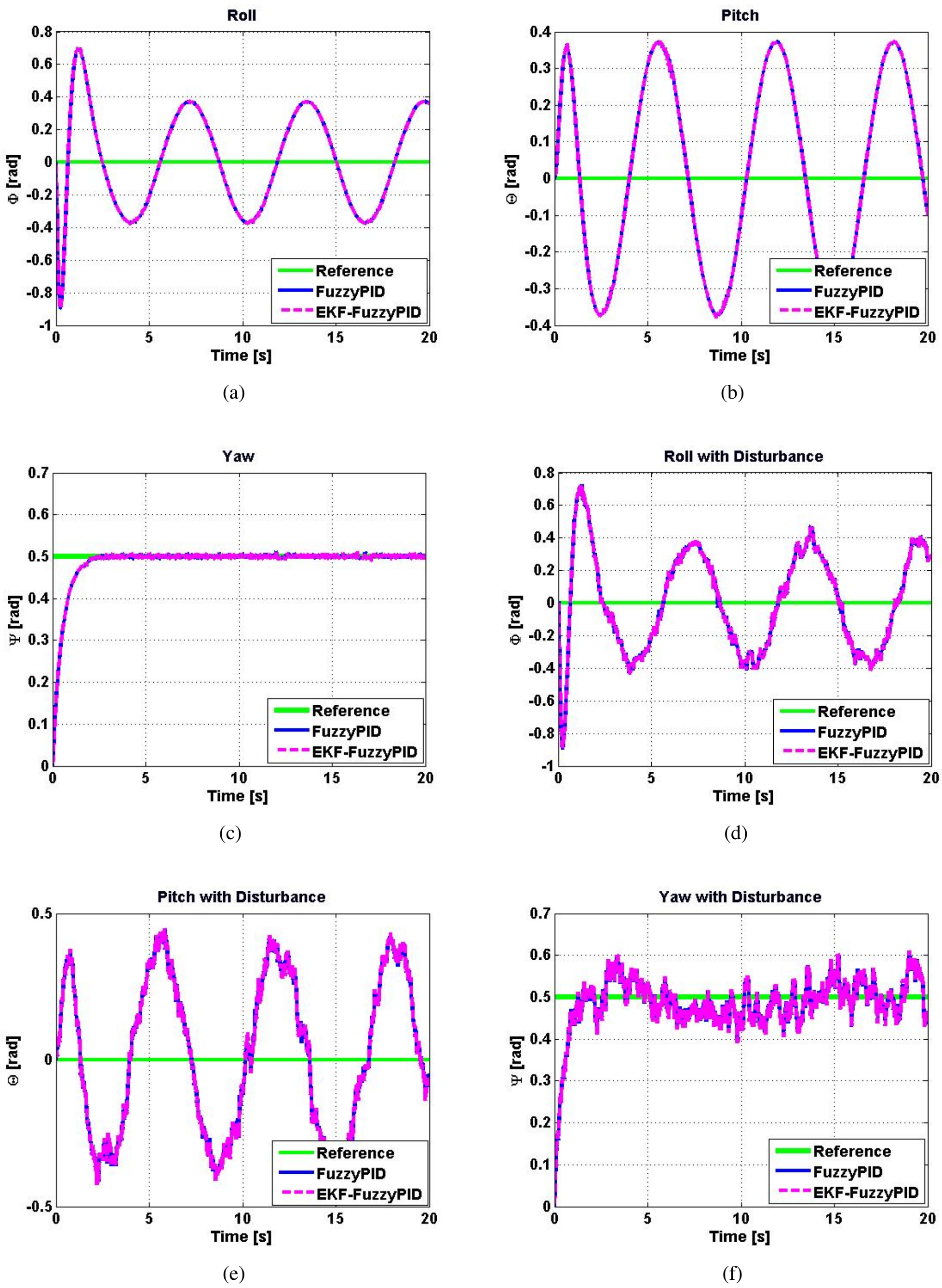

Figure 9: Angular position response: (a) roll, (b) pitch, (c) yaw, (d) roll with disturbance, (e) pitch with disturbance, (f) yaw with disturbance

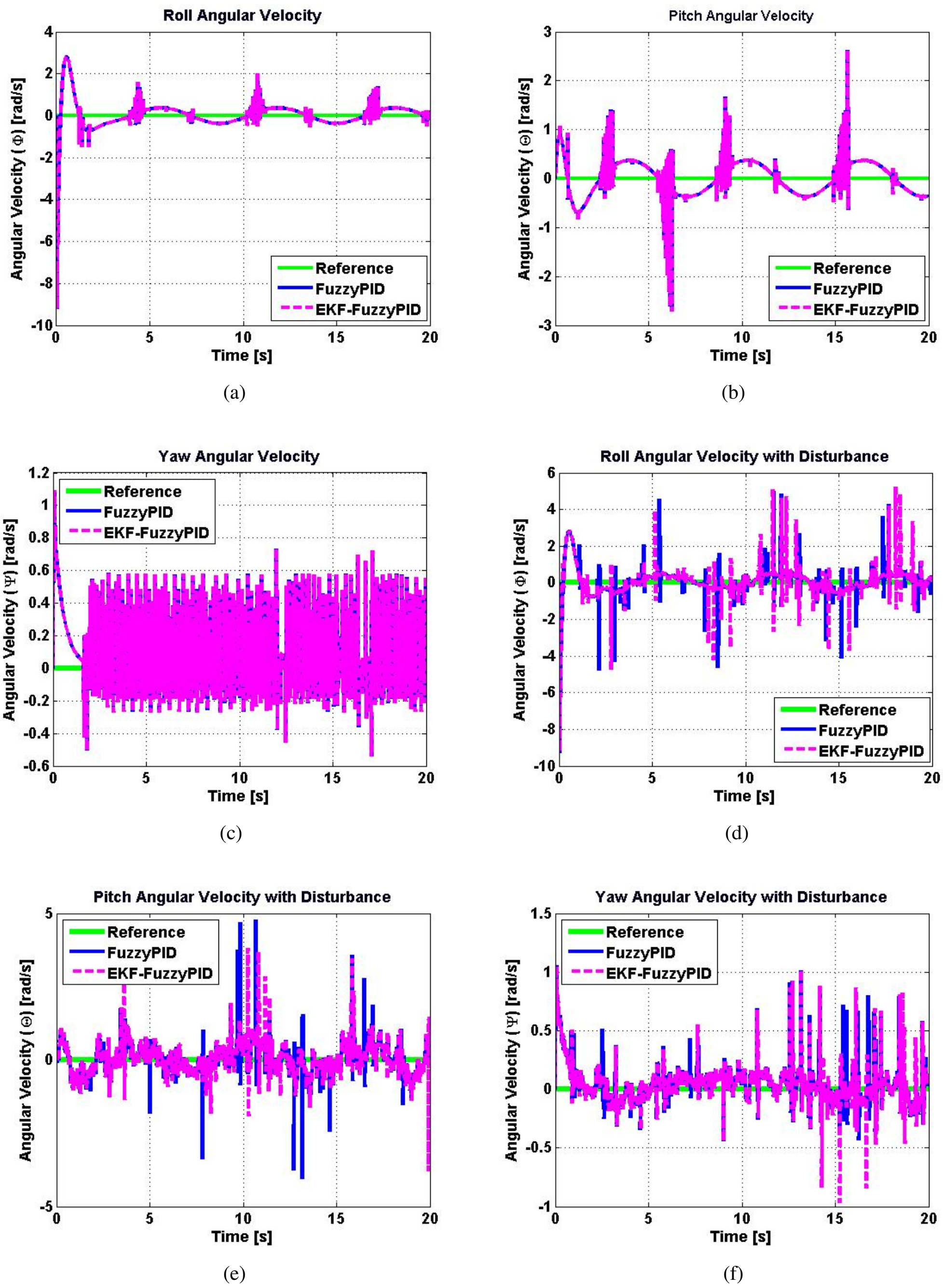

Figure 10: Angular velocity response: (a) velocity of roll, (b) velocity of pitch, (c) velocity of yaw , (d) velocity of roll with disturbance, (e) velocity of pitch with disturbance, (f) velocity of yaw with disturbance

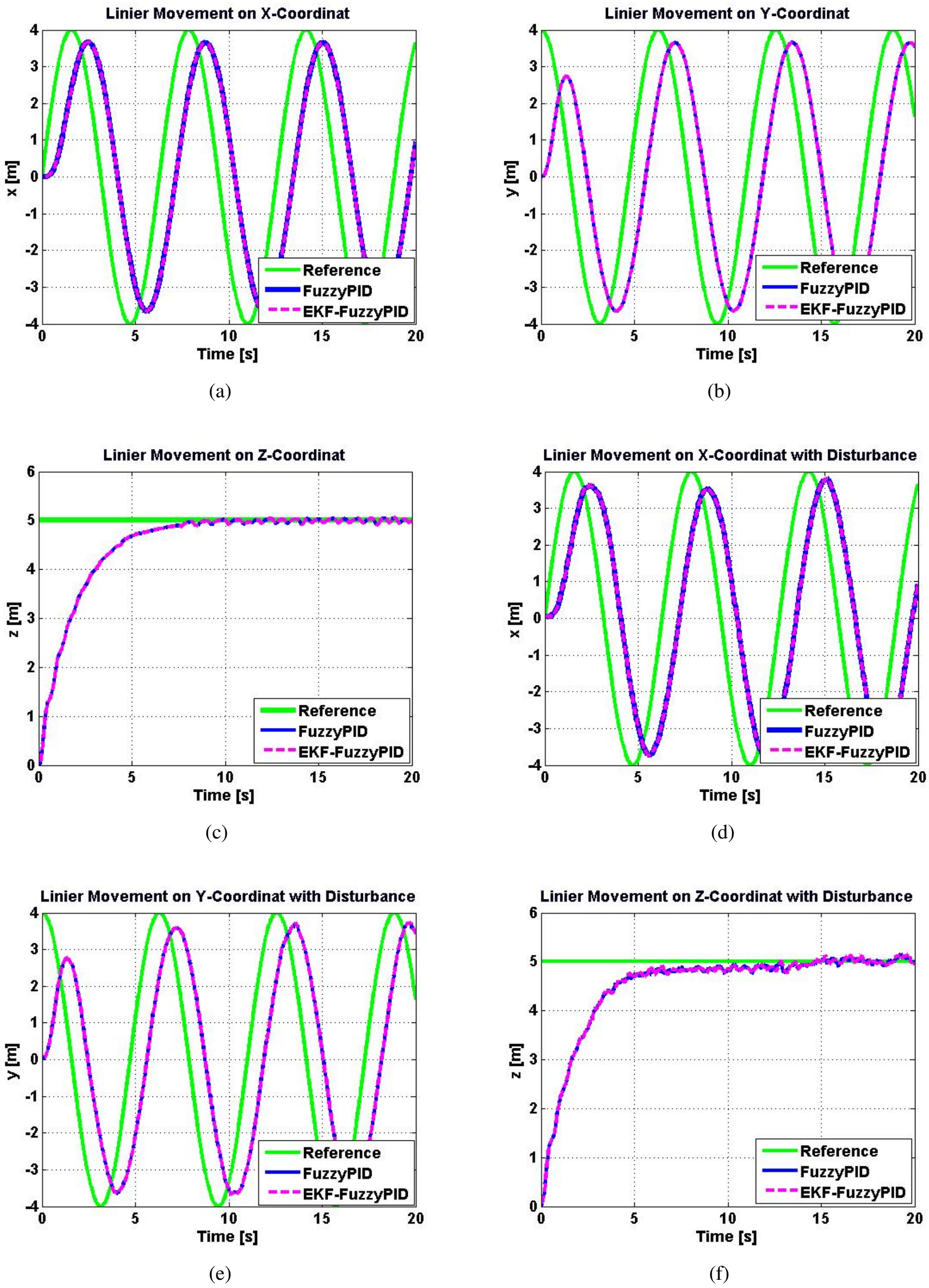

Figure 11: Linear position response: (a) x, (b) y, (c) z, (d) x with disturbance, (e) y with disturbance, (f) z with disturbance

The settling time for the x as well as y remains undefined (NaN), but the settling time for z increases to 19.7341 seconds, indicating that the disturbance worsens the time required to achieve stability in the z axis. Steady-state errors in x, y, and z slightly increased to 2.7114, 1.8128, and 0.0494, respectively, reflecting that the perturbation worsened the final position error in all axes, although the z-axis still performed better than x and y. Overall, although the system was able to control the position better in the z-axis, the perturbation worsened the performance in the other axes, both in overshoot and steady-state error.

Additional analysis of Figure 11 shows that on the x-axis (Fig. 11a and 11d), both Fuzzy-PID and EKF-Fuzzy-PID show amplitudes of about 4 meters with nearly identical frequencies (0.15 Hz); however, Fuzzy-PID lags behind the reference by about 1.5 seconds, while EKF-Fuzzy-PID exhibits almost no time shift. On the y-axis (Fig. 11b and 11e), Fuzzy-PID experiences about 3 seconds phase delay, while EKF-Fuzzy-PID actually leads the reference by about 0.5 seconds, reflecting an advantage in lateral position tracking. For the z-axis (Fig. 11c and 11f), significant differences are seen in stability and accuracy. Fuzzy-PID experiences an overshoot of 3.7 m and does not reach stability, with a final oscillation continuing, while EKF-Fuzzy-PID produces an overshoot of 4.9 m but is able to settle down in 4 s and achieve a final error close to zero. These results indicate that although there is a slight increase in overshoot in EKF-Fuzzy-PID, the overall performance in terms of stability and precision is much superior to Fuzzy-PID, especially under disturbed conditions.

The analysis of the EKF-FuzzyPID control system in Figure 12 shows significant instability both in the undisturbed condition and with disturbances in velocities. In the undisturbed system, the overshoot in the x, y, and z velocities is undefined (Inf), indicating a very large and uncontrolled system response in the early stage. The settling time for all three axes is also undefined (NaN), indicating that the system does not reach stability within a certain time. The steady-state errors for velocities are 3.5232 in x, 0.9642 in y, and 0.3326 in z, showing that the final position error is relatively large, especially in the x, with smaller errors in the y and z axes. In the disturbed condition, the overshoot remains undefined (Inf) in all three axes, and the settling time also remains undefined (NaN), indicating that the disturbance worsens the stability of the system. The steady-state error at x velocity increases to 3.1306, while at y and z it increases slightly to 1.0171 and 0.2569, indicating that the disturbance worsens the steady-state error, especially at the x-axis. Overall, although the disturbance worsens the system performance, the error at x velocity remains quite high, while the y and z axes show better stability improvement compared to x, although there is still an increase in steady-state error at all axes.

Quantitative analysis of Figure 12 shows that in both Fig. 12a and 12b, the Fuzzy-PID signal has an amplitude of about 3.5 m/s with a frequency of 0.15 Hz, but lags behind the EKF-Fuzzy-PID by about 3 s in phase, which is almost parallel to the reference. This indicates that the EKF-Fuzzy-PID is able to provide more precise and responsive linear velocity tracking. In Fig. 12c (Vz), the Fuzzy-PID shows an overshoot of about 4 m/s, 0.2 m/s lower than the EKF-Fuzzy-PID and remains oscillating without obvious stability, while the EKF-Fuzzy-PID is able to reach stability in about 4 s with a steady-state error close to zero. Under disturbed conditions (Fig. 12d–f), similar patterns are still visible: in the x and y axes, the amplitude and frequency characteristics are relatively similar to those of the undisturbed condition, but the phase difference remains consistent, indicating the superiority of the EKF in time response. In the z-axis (Fig. 12f), in the Fuzzy-PID method, the system response is still dominated by prolonged oscillations. In contrast, the system with EKF-Fuzzy-PID still shows stability even though there is an increase in signal variability after reaching steady state, which is likely caused by random disturbances." Overall, the EKF-Fuzzy-PID approach successfully minimizes phase delay, accelerates the process towards stability, and maintains linear velocity accuracy more consistently than conventional methods.

In some conditions when the system is disturbed, the final stability has not been achieved during the simulation duration, so the time to reach steady state cannot be determined with certainty. This is due to the continuous and random nature of the disturbance, resembling wind turbulence in the real world, which makes the system continuously re-estimate and adjust the

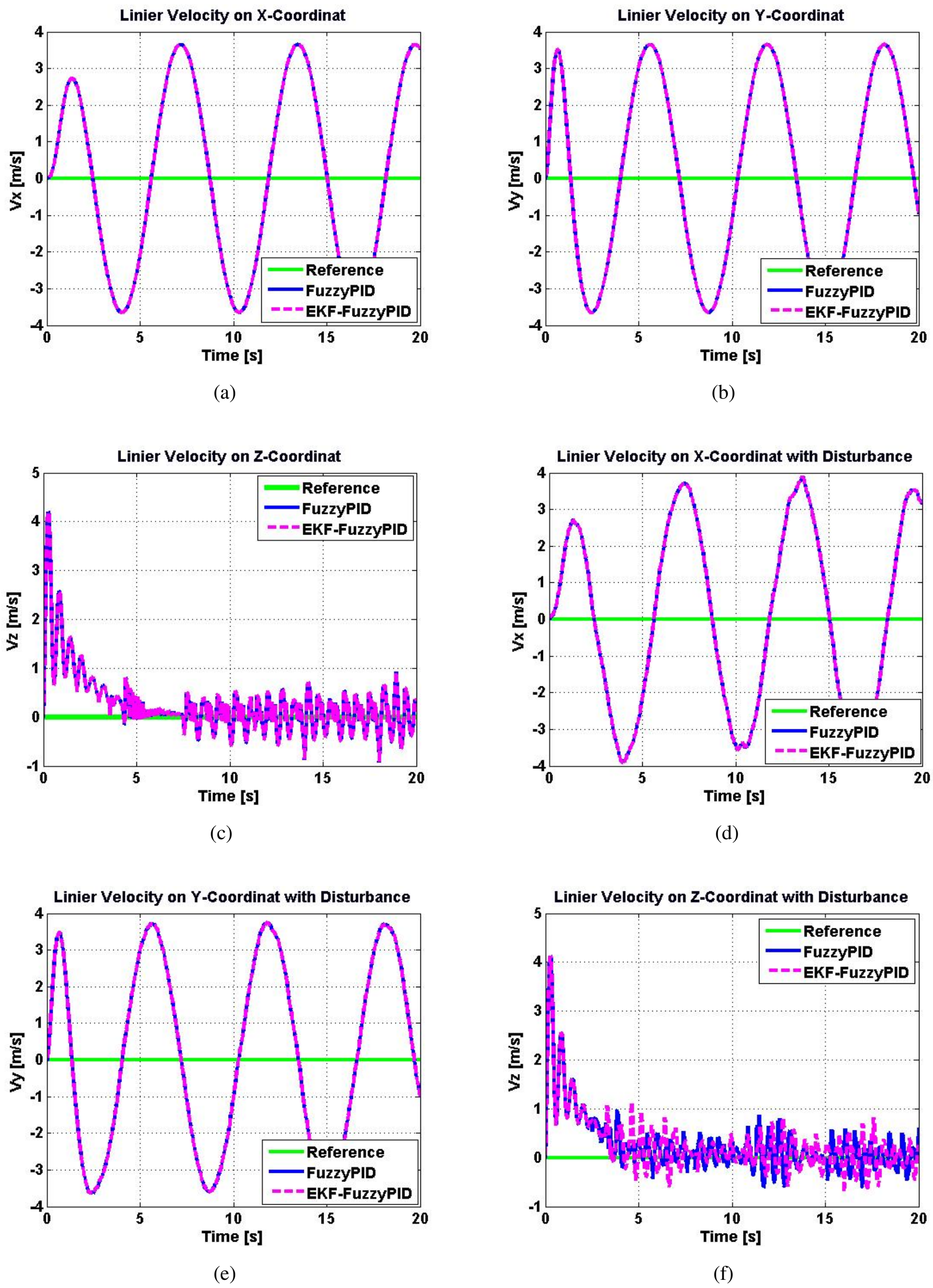

Figure 12: Linear velocity response: (a) velocity of x , (b) velocity of y, (c) velocity of z, (d) velocity of x with disturbance, (e) velocity of y with disturbance, (f) velocity of z with disturbance

control to maintain stability.

For angular velocity data, although the graph shows that the system is able to reach the set point, it is important to note that the EKF-based Fuzzy-PID significantly reduces the initial transient fluctuations. This indicates that the system is able to dampen disturbances quickly. At linear velocity, the system has the capability to reach the reference value and shows stability. It is evident that the integration of EKF in fuzzy tuning results in more precise control even when sudden disturbances occur. For trajectory tracking, linear position of z has the maximum error 0.1 m after 10 seconds of simulation. This indicates that the system is able to maintain position with high accuracy and is adaptive to variations in environmental conditions.

5. Conclusion

This research evaluates the performance of the EKF-FuzzyPID on a quadcopter in various scenarios, both without disturbances and with disturbances. Overall, the results of analysis indicates that the system has good ability to follow the trajectory reference, especially in undisturbed conditions. The system is able to follow the reference with high precision, with position errors of no more than 0.15 m. In addition, the steady-state error on several variables, such as yaw angle and z position, shows a relatively small value, indicating that the system is still able to achieve the reference value with good accuracy in several aspects.

However, there are some limitations in the system performance, especially in handling undefined overshoot on the speed and position of the x and y axes. The settling time on most variables is also undefined, indicating that the system has difficulty in reaching a steady state, especially in conditions with disturbances. As shown in Figure 8b, despite the increase in deviation at the beginning of the response due to disturbances, the system can quickly adapt and return to following the reference, with an average increase in position error of about 0.09 m for each axis. However, in some cases, external disturbances cause an increase in steady-state error as well as overshoot, especially in the x and yaw axes.

These results indicate that although EKF-FuzzyPID enhance the stability of quadcopter control, additional strategies are needed to overcome the problems of overshoot and undefined settling time, especially in dynamic and disturbed environments. To improve the overall system performance, optimization of control parameters or integration of adaptive methods can be implemented..

Acknowledgments

The support of Department of Mathematics, Institut Teknologi Sepuluh Nopember is gratefully acknowledged.

References

Abdelhay S. & Zakriti A. 2019. Modeling of a quadcopter trajectory tracking system using PID controller. *Procedia Manufacturing* **32**: 564–571.

Arghavani N., Almobaied M., Guzelkaya M. & Eksin I. 2017. On-line rule weighting for PID-type fuzzy logic controllers using extended Kalman filter. *IFAC-PapersOnLine* **50**(1): 6946–6951.

Aydenlou H.R. & Subasi A. 2025. Designing a fuzzy-based PID controller for separation control in the backward-facing step flow. *International Communications in Heat and Mass Transfer* **167**: 109144.

Chang X., Jin C. & Cheng Y. 2024. Dynamics and advanced active disturbance rejection control of tethered UAV. *Applied Mathematical Modelling* **135**: 640–665.

Gautam D. & Ha C. 2013. Control of a quadrotor using a smart self-tuning fuzzy PID controller. *International Journal of Advanced Robotic Systems* **10**(11): 380.

He F., Zhao Y., Zhao L., Wu X., Dong W., Xie S. & He C. 2025. Transient behavior of fuzzy PID-controlled transpiration cooling with phase change under dynamic thermal environments. *International Journal of Thermal Sciences* **217**: 110088.

Honarbari A., Najafi-Shad S., Saffari Pour M., Ajarostaghi S.S.M. & Hassannia A. 2021. MPPT improvement for PMSG-based wind turbines using extended Kalman filter and fuzzy control system. *Energies* **14**(22): 7503.

Issa H.A., Abdali L.M., Alhusseini H. & Velkin V.I. 2025. Design, modeling, and control of a dual-axis solar tracker using fractional order PID controllers for enhanced energy efficiency. *Results in Engineering* **27**: 106073.

Iza B.A., Fiddina Q.A., Fadhilah H.N., Arif D.K. & Mardlijah. 2022. Automatic Guided Vehicle (AGV) tracking model estimation with ensemble Kalman filter. *AIP Conference Proceedings* **2641**(1): 030019.

Jiang Y. 2022. Study on eigenvalue and eigenvector introduction. *Journal of Physics: Conference Series* **2282**(1): 012004.

Lalwani C.S., Disney S.M. & Towill D.R. 2006. Controllable, observable and stable state space representations of a generalized order-up-to policy. *International Journal of Production Economics* **101**(1): 172–184.

Mardlijah, Akbar Y.F. & Iza B.A. 2023. Comparative analysis of SMC and FSMC on Autonomous Underwater Vehicle (AUV) with active ballast. *Proceedings of the 2023 International Conference on Computer, Control, Informatics and its Applications*, pp. 7–12.

Mellodge P. 2016. *A Practical Approach to Dynamical Systems for Engineers*. Oxford: Woodhead Publishing.

Nguyen A.T., Nguyen N.H. & Trinh M.L. 2025. Fuzzy PD control for a quadrotor with experimental results. *Results in Control and Optimization* **19**: 100568.

Nippatla V.R. & Mandava S. 2025. Performance analysis of permanent magnet synchronous motor based on transfer function model using PID controller tuned by Ziegler-Nichols method. *Results in Engineering* **26**: 105460.

Odry Á., Kecskes I., Sarcevic P., Vizvari Z., Toth A. & Odry P. 2020. A novel fuzzy-adaptive extended Kalman filter for real-time attitude estimation of mobile robots. *Sensors* **20**(3): 803.

Oloo J.O. 2021. Design of extended Kalman filter optimized fuzzy PID controller for a quadcopter in the event of one rotor failure. Master's thesis. Jomo Kenyatta University of Agriculture and Technology.

Pandey A.K., Singh V. & Jain S. 2022. Study and comparative analysis of perturb and observe (P&O) and fuzzy logic based PV-MPPT algorithms. In Shaw R.N., Ghosh A., Mekhilef S. & Balas V.E. (eds.). *Applications of AI and IOT in Renewable Energy*: 193-209. Amsterdam: Academic Press/Elsevier.

Şahin İ. & Ulu C. 2023. Altitude control of a quadcopter using interval type-2 fuzzy controller with dynamic footprint of uncertainty. *ISA Transactions* **134**: 86–94.

Somwanshi D., Bundele M., Kumar G. & Parashar G. 2019. Comparison of fuzzy-PID and PID controller for speed control of DC motor using LabVIEW. *Procedia Computer Science* **152**: 252–260.

Szedlak-Stinean A.I., Precup R.E., Petriu E.M., Roman R.C., Hedrea E.L. & Bojan-Dragos C.A. 2022. Extended Kalman filter and Takagi-Sugeno fuzzy observer for a strip winding system. *Expert Systems with Applications* **208**: 118215.

Taghavifar H. 2021. EKF estimation based PID Type-2 fuzzy control of electric cars. *Measurement* **173**: 108557.

Truong D.Q. & Ahn K.K. 2011. Force control for press machines using an online smart tuning fuzzy PID based on a robust extended Kalman filter. *Expert Systems with Applications* **38**(5): 5879–5894.

Wang L., Horn B.K.P. & Strang G. 2017. Eigenvalue and eigenvector analysis of stability for a line of traffic. *Studies in Applied Mathematics* **138**(1): 103–132.

Wang T., Wang H., Hu H., Lu X. & Zhao S. 2022. An adaptive fuzzy PID controller for speed control of brushless direct current motor. *SN Applied Sciences* **4**(3): 71.

Zaman U., Junaid K., Ku J., Kim S., Lee E. & Kim K. 2025. Trajectory optimization and control of autonomous surface ships in dynamic environments using a hybrid extended Kalman filter and fuzzy logic system. *Proceedings of the 2025 International Conference on Artificial Intelligence in Information and Communication*, pp. 0395–0401. IEEE.

Zhu Z., Liu Y., He Y., Wu W., Wang H., Huang C. & Ye B. 2022. Fuzzy PID control of the three-degree-of-freedom parallel mechanism based on genetic algorithm. *Applied Sciences* **12**(21): 11128.

Department of Mathematics
Faculty of Science and Data Analytics
Institut Teknologi Sepuluh Nopember
Kampus ITS Sukolilo 60111
Surabaya, INDONESIA
*E-mail: 7002222003@student.its.ac.id, cha_imron15@its.ac.id, mardlijah@its.ac.id**

Received: 9 June 2025
Accepted: 31 August 2025

*Corresponding author